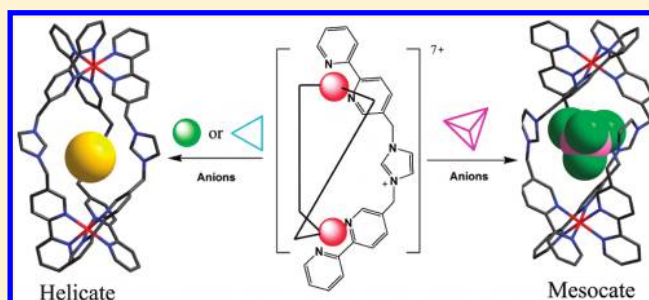


Anion-Dependent Formation of Helicates versus Mesocates of Triple-Stranded M_2L_3 ($M = Fe^{2+}, Cu^{2+}$) ComplexesFengjuan Cui,^{†,‡} Shaoguang Li,^{†,‡} Chuandong Jia,^{†,‡} Jennifer S. Mathieson,[§] Leroy Cronin,[§] Xiao-Juan Yang,[†] and Biao Wu^{*,†}[†]State Key Laboratory for Oxo Synthesis & Selective Oxidation, Lanzhou Institute of Chemical Physics, CAS, Lanzhou 730000, China[‡]Graduate University of Chinese Academy of Sciences, Beijing 100049, China[§]WestCHEM, School of Chemistry, The University of Glasgow, University Avenue, Glasgow G12 8QQ, Scotland, U.K.

Supporting Information

ABSTRACT: A series of dinuclear triple-stranded complexes, $[Fe_2L_3\supset X]X_6$ [$X = BF_4^-$ (1), ClO_4^- (2)], $[Fe_2L_3\supset SO_4]_2(SO_4)_5$ (3), $[Fe_2L_3\supset Br](BPh_4)_6$ (4), $Fe_2L_3(NO_3)Br_6$ (5), and $[Cu_2L_3\supset NO_3](NO_3)_6$ (6), which incorporate a central cavity to encapsulate different anions, have been synthesized via the self-assembly of iron(II) or copper(II) salts with the *N,N'*-bis-[5-(2,2'-bipyridyl)methyl]imidazolium bromide (LBr) ligand. X-ray crystallographic studies (for 1–4 and 6) and elemental analyses confirmed the cage-like triple-stranded structure. The anionic guest is bound in the cage and shows remarkable influence on the outcome of the self-assembly process with regard to the configuration at the metal centers. The mesocates (with different configurations at the two metal centers) have formed in the presence of large tetrahedral anions, while helicates (with the same configuration at both metal centers) were obtained when using the relatively smaller spherical or trigonal-planar anions Br^- or NO_3^- .



INTRODUCTION

Helix is an important structural motif in nature. Dinuclear triple-stranded $[M_2L_3]$ complexes, as simple models for more complex natural structures of biological molecules, have been of much interest.¹ For example, the diiron complex of rhodoturlic acid can help one to understand how a siderophore controls iron uptake in microorganisms.^{1b} Another aspect is that these model systems can mimic essential biological processes such as bacterial photosynthesis and respiration.^{1c} On the other hand, these complexes also provide important information to the study of the structure, function, and chirality control in metallosupramolecular chemistry. Intense research activities have focused on the synthesis of correlative topologically interesting derivatives, including two-dimensional racks,^{1d} ladders^{1e} and grids,^{1f} and intertwined catenanes and knots,^{1g,h} as well as on the introduction of specific magnetic, electronic, and spectroscopic properties into the complexes to develop functional materials.^{1k}

Various ligands such as bis(bipyridine),^{1c,2} dicatechol,³ benzimidazole⁴ and the recently reported bis(dipyrromethene)⁵ have been employed to construct the triple-stranded $[M_2L_3]$ complexes. According to the chirality at each six-coordinated metal center, dinuclear $[M_2L_3]$ complexes may exhibit three stereospecial configurations— $\Delta\Delta$, $\Lambda\Lambda$, and $\Delta\Lambda$ —which result in two possible architectures when using achiral ligands: homochiral helicates ($\Delta\Delta$ or $\Lambda\Lambda$) and achiral mesocates ($\Delta\Lambda$).⁶ The helicate structures were reported in as early as 1978,^{1b} but the

first mesocate was only structurally characterized almost 20 years later.^{3b} Nevertheless, ever since the report of this mesocate complex, chemists have devoted many efforts to understanding the formation of helicates versus mesocates and to achieving high stereoselectivity of triple-stranded coordination complexes.⁶ For instance, Raymond et al.⁷ observed helicates and mesocates with bis(hydroxypyridinone) in thermodynamic equilibrium in solution. Albrecht et al.^{3b,6d} proposed an empirical *odd–even* rule, which demonstrates that the spacer of the ligand plays an important role in the formation of helicates or mesocates. Recently, the Dolphin group^{5b} successfully synthesized and isolated both helicates and mesocates by using bis(dipyrromethene) with a single methylene spacer. However, control of the formation of the two isomers still remains a challenge.

It has been reported that some cations (e.g., Li^+ , Na^+ , and K^+) can template the synthesis of triple-stranded $[M_2L_3]$ structures.⁸ In contrast, the anion-controlled self-assembly of $[M_2L_3]$ metal helicates or mesocates is rare despite the intensive investigations of anion binding and anion coordination in the past 2 decades.⁹ To the best of our knowledge, the only example of anion-induced resolution of helicates and mesocates was reported by Kruger and co-workers,^{2d} who observed the selective formation of helicates by using the relatively small chloride ion. Moreover, the Rice group¹⁰ reported that the trigonal-planar

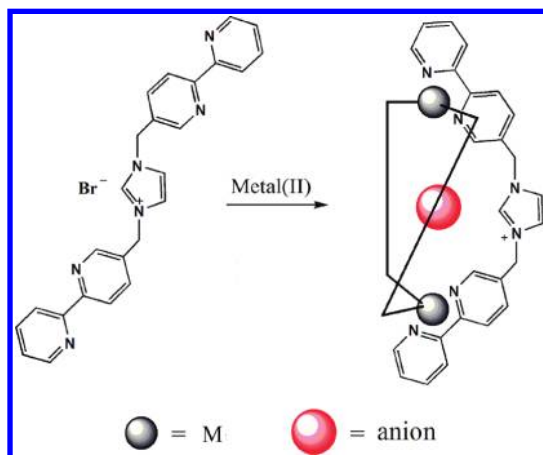
Received: July 4, 2011

Published: November 30, 2011

NO_3^- anion, rather than the tetrahedral ClO_4^- , can lead to the major C_3 head-to-head (HHH) isomer in the triple helicate $[\text{Co}_2\text{L}_3]^{4+}$ with unsymmetrical chiral ligands in solution. In the self-assembly of metallosupramolecular architectures, anions have also been found to be capable of directing the formation of a variety of ordered structures, such as the circular pentanuclear double helicate structure,¹¹ mercurocarborand,¹² molecular squares,¹³ $[\text{M}_4\text{L}_6]$ cages,¹⁴ and rotaxanes.¹⁵ On the basis of these results, the anion-templated stereoselective synthesis of triple metal helicates or mesocates might be achieved when incorporating proper anion-binding sites to the ligand. Additionally, because the highly charged cagelike complexes contain an electropositive central cavity where anions can be encapsulated, these complexes would be potential anion receptors for studying host–guest chemistry and anion recognition.

In this work, we designed a heterotopic ligand (LBr) containing the bis(bipyridyl) metal coordination sites and the imidazolium bridge that is a potential anion-binding group. Previously, we have synthesized a number of anion receptors including metal coordination-assisted anion-binding systems.¹⁶ Herein we describe the formation of both triple-stranded helicates and mesocates from LBr and divalent metals (Chart 1). Very

Chart 1

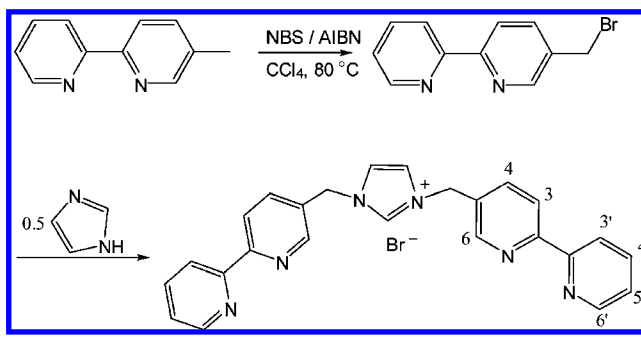


interestingly, selective crystallization of the anion-encapsulating helicate or mesocate can be modulated by the size and/or shape of the anion: the smaller anions (Br^- and NO_3^-) tend to template the helicate structure, while the larger tetrahedral anions (BF_4^- , ClO_4^- , and SO_4^{2-}) favor the mesocate isomer. The changes of the ligand conformation upon the binding of anions of different size or shape may be responsible for the selectivity observed in the two cases.

RESULTS AND DISCUSSION

Synthesis and Crystal Structure of the Ligand LBr. The ligand LBr was prepared through modification of the general synthetic method reported previously in the literature,¹⁷ as outlined in Scheme 1. The reaction of 5-(bromomethyl)-2,2'-bipyridine and imidazole in MeCN gave the desired product as a white powder in 51% yield, with the Br^- ion as the counteranion. The ligand is soluble in H_2O , dimethyl sulfoxide (DMSO), *N,N*-dimethylformamide (DMF), methanol (MeOH), and acetonitrile and slightly soluble in ethanol (EtOH) and dichloromethane. The bromide salt LBr crystallizes as colorless block

Scheme 1. Synthesis of the Ligand LBr



crystals [space group $P2(1)/c$] from a CH_3OH solution. The imidazolium ring links two bipyridyl (bpy) units through methylene groups and is coplanar with the two $-\text{CH}_2-$ groups (Figure 1). The ligand molecule adopts an “S” conformation,

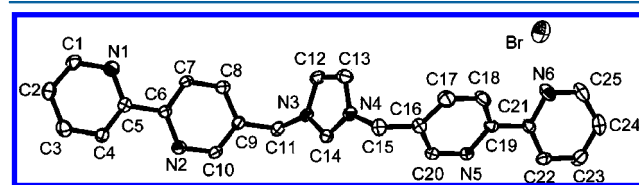


Figure 1. Molecular structure of LBr (thermal ellipsoids at the 30% probability level; H atoms were omitted for clarity).

and the bond angles of the spacer $\text{C}_{\text{bipy}}-\text{C}_{\text{CH}_2}-\text{N}_{\text{imd}}$ are 112.2° and 117.1° , respectively. The mean C–N bond length of the imidazolium is 1.326 \AA .

Synthesis of the Complexes. The iron(II) complex $[\text{Fe}_2\text{L}_3\text{O}(\text{BF}_4)](\text{BF}_4)_6$ (1) was synthesized by mixing the aqueous solutions of LBr and $\text{FeBr}_2 \cdot 6\text{H}_2\text{O}$ followed by treatment with NaBF_4 . In the same way, the complexes $[\text{Fe}_2\text{L}_3\text{O}(\text{ClO}_4)](\text{ClO}_4)_6$ (2), $[\text{Fe}_2\text{L}_3\text{O}(\text{SO}_4)]_2(\text{SO}_4)_5$ (3), and $[\text{Fe}_2\text{L}_3\text{O}(\text{Br})](\text{BPh}_4)_6$ (4) were obtained in the presence of NaClO_4 , Na_2SO_4 , or NaBPh_4 . It is noteworthy that the Br^- ion is included in the cage in the solid-state structure of 4 rather than the much larger BPh_4^- anion when using sodium tetraphenylborate to exchange with the Br^- ion, which is different from the other cases. The nitrate-including complex $\text{Fe}_2\text{L}_3(\text{NO}_3)\text{Br}_6$ (5) was obtained through the reaction of LBr with iron(III) nitrate in the presence of excess iron powder, while the dicopper(II) complex $[\text{Cu}_2\text{L}_3\text{O}(\text{NO}_3)](\text{NO}_3)_6$ (6) was directly synthesized from LBr and copper(II) nitrate. These dinuclear complexes were isolated in quantitative or close to quantitative yield and were fully characterized by elemental analysis, IR spectroscopy, and X-ray crystallography (for 1–4 and 6). The elemental analysis results are consistent with the formation of dinuclear species of the general formula $[\text{M}_2\text{L}_3]^{7+}$ (Chart 1), and there is no evidence for the occurrence of other stoichiometries. The compounds are sparingly soluble in water, MeOH, and acetonitrile and would decompose in higher polar solvents such as DMSO and DMF. Electrospray ionization mass spectrometry (ESI-MS) spectra were recorded, and complexes 1, 2, 4, and 5 displayed the $[\text{M}_2\text{L}_3\text{X}_5]^{2+}$ ($\text{X} = \text{anion}$) species with the expected isotopic distribution patterns of the dinuclear complexes (Figure S3 in the Supporting Information). The sulfate-including complex 3 and the copper(II) complex 6 showed only the $[\text{M}_2\text{L}_2]$ fragments. The former case might be due to the poor solubility of

complex **3**, which decomposes at low concentrations, while the latter may be explained by the fact that the Cu^{II} ion disfavors the octahedral coordination and the triple helicate might have disassembled in solution. Moreover, the spectrum of complex **5** with the composition $\text{Fe}_2\text{L}_3(\text{NO}_3)\text{Br}_6$, as demonstrated by elemental analysis, showed a series of M_2L_3 fragments with mixed anions. The iron(II) complexes **1** and **5**, which exhibit the mesocate and helicate structures, respectively, were employed as typical examples to study the solution configuration by ^1H and ^{13}C NMR experiments.

Solid-State Structures of Complexes 1–4 and 6. The crystal structures and anion-binding modes of the complexes $[\text{Fe}_2\text{L}_3(\text{BF}_4)](\text{BF}_4)_6 \cdot 3\text{CH}_3\text{CN}$ (**1**), $[\text{Fe}_2\text{L}_3(\text{ClO}_4)](\text{ClO}_4)_6 \cdot 3\text{CH}_3\text{CN}$ (**2**), $[\text{Fe}_2\text{L}_3(\text{SO}_4)]_2(\text{SO}_4)_5 \cdot 3\text{CH}_3\text{CN}$ (**3**), $[\text{Fe}_2\text{L}_3(\text{Br})](\text{BPh}_4)_6 \cdot 6\text{CH}_3\text{CN}$ (**4**), and $[\text{Cu}_2\text{L}_3(\text{NO}_3)](\text{NO}_3)_6$ (**6**) were investigated by single-crystal X-ray diffraction. Deep-red crystals of the iron(II) compounds $[\text{Fe}_2\text{L}_3]^{7+}$ (**1–4**) and blue block crystals of the copper(II) complex **6** were obtained by the slow diffusion of ether into a CH_3CN solution of the corresponding complex at room temperature for about 2 weeks. All of the complexes show a ligand-to-metal ratio of 3:2, and all of the crystals have the same habit and appearance, crystallizing in the trigonal space group $R\bar{3}$, with the individual Fe or Cu centers lying on 3-fold special positions and the ligands being arranged around a 3-fold axis. Notably, both the helicates and mesocates are in the same space group, which is different from some reported cases, in which the two isomers show different space groups.^{5b} The complexes feature the typical octahedral bipyridine–metal coordination at both sides of the ligands, leading to a central cage to accommodate an anion. The imidazolium functionality offers electrostatic interactions or $(\text{C}-\text{H})^+ \cdots \text{X}^-$ -type ionic hydrogen-bonding interactions with the encapsulated anion. The two C–N distances of the imidazolium ring of a given ligand are slightly different (except for the perchlorate complex **2**, in which the two C–N distances are equal), and the mean C–N distance (1.335 Å) in the iron(II) complexes is slightly longer than that in the ligand (1.326 Å) and in the copper(II) complex **6** (1.284 Å).

$[\text{Fe}_2\text{L}_3\supset(\text{BF}_4)](\text{BF}_4)_6 \cdot 3\text{CH}_3\text{CN}$ (**1**). The tetrafluoroborate complex **1** consists of a cationic cage capsule $[\text{Fe}_2\text{L}_3\supset\text{BF}_4]^{6+}$, six BF_4^- counteranions, and three solvent CH_3CN molecules. Three ligands adopt the “pseudo-C” conformations and form a triple-stranded dinuclear structure with two Fe^{II} ions. The Fe atoms in the two $[\text{Fe}(\text{bpy})_3]^{2+}$ units show a Δ configuration at one side and a Λ configuration at the other side, indicating a mesocate structure. A cavity bound by the two $[\text{Fe}(\text{bpy})_3]$ head groups and separated by ca. 10.6 Å (Fe \cdots Fe distance) can be identified, which is formed by three surrounding imidazolium rings with a ca. 6.7 Å separation between each other. The two bpy moieties in one ligand head to the same orientation, leading to lower symmetry of the ligand (Figure S4 in the Supporting Information). One tetrafluoroborate ion is encapsulated in the highly charged central cavity to form the capsule $[\text{Fe}_2\text{L}_3\supset\text{BF}_4]^{6+}$, which is also demonstrated by the ^{19}F NMR spectrum (Figure S7 in the Supporting Information). The encapsulated BF_4^- anion occupies the center of the cage and interacts with the three ligands via three hydrogen bonds from the 6-CH groups of the bpy subunits, which have been activated through metal coordination (Figure 2a). Notably, all three C–H \cdots F bonds [C10 \cdots F2, 2.999(3) Å] point to the same F atom (F2), which sits at the C_3 axis, while the other three C_3 -related F atoms are not involved in hydrogen bonding (Table 1).

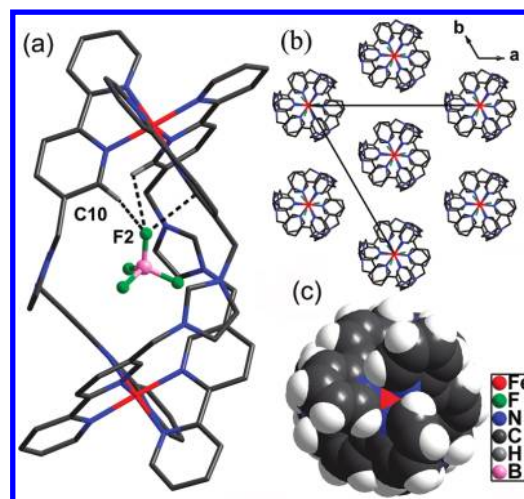


Figure 2. (a) Molecular structure of the cationic unit ($\Delta\Lambda$)- $[\text{Fe}_2\text{L}_3\supset\text{BF}_4]^{6+}$ of **1**. Noninteracting H atoms and external counteranions were omitted for clarity. (b) Packing diagram of **1** viewed from the c axis showing the arrangement of seven neighboring complexes. (c) Space-filling depiction viewed down the C_3 axis.

Unexpectedly, in the structure of **1**, the imidazolium CH^+ moieties do not participate in the $\text{CH}^+ \cdots \text{X}^-$ -type ionic hydrogen bonds with the encapsulated anion; instead, the imidazolium planes are oriented in the tangent direction (i.e., the “wall” of the cage). As a result, the CH^+ vector forms a very acute C–H \cdots F angle (63.4°) with the three “free” F atoms of the BF_4^- anion, although the C \cdots F distance is quite short [3.108(5) Å]. This is remarkably different from a related complex with imidazolium groups, which features three C–H \cdots Br $^-$ hydrogen bonds between the imidazolium groups and the encapsulated Br $^-$ anion besides the C–H \cdots Br interactions from the bpy units.¹⁸ In the helicate complexes **4** and **6** (vide infra) reported herein, the nitrate or bromide ion also forms this C–H \cdots X $^-$ hydrogen bond. The absence of C–H \cdots Br $^-$ interactions in the current case may be attributed to the larger tetrahedral BF_4^- anion, which forces the imidazolium planes to rotate away. Therefore, the binding of the BF_4^- anion might have been achieved by a combination of hydrogen-bonding and electrostatic attractions. A packing diagram (Figure 2b) of **1** indicates that every one cage complex is surrounded by six neighbors via interactions with the external BF_4^- anions.

$[\text{Fe}_2\text{L}_3\supset(\text{ClO}_4)](\text{ClO}_4)_6 \cdot 3\text{CH}_3\text{CN}$ (**2**). As an isomorphous complex of the tetrafluoroborate analogue **1**, the skeletal structure of the perchlorate complex **2** consists of two Fe^{II} ions, three L molecules, and one encapsulated perchlorate anion, forming the highly charged $[\text{Fe}_2\text{L}_3\supset\text{ClO}_4]^{6+}$ cage, as well as the other six ClO_4^- ions as counterions. There are also three $\text{C}_{\text{py}}-\text{H} \cdots \text{O}$ hydrogen bonds [C10 \cdots O2, 3.108(3) Å] between the encapsulated perchlorate anion and the bpy subunits (Table 1). The ligands with the “pseudo-C” shape lead to different configurations at the two metals (the mesocate structure) as well (Figure 3). The three ligand strands wrap around the two metals and adopt a conformation, with the carbenic C atoms pointing aside and deviating from the central anion. This orientation results in too small angles (62.1°) to define any C–H \cdots X $^-$ hydrogen bonding between the perchlorate anion and the imidazolium CH^+ moieties [C14 \cdots O1, 3.102(5) Å]. Hence, the perchlorate ion should also be bound by hydrogen-bonding and strong electrostatic interactions as in **1**. In the structure of **2**, the bridging groups on the ligands constrain a Fe \cdots Fe distance of

Table 1. Hydrogen-Bonding Parameters (Å and deg) around the Encapsulated Anions in the Complexes

anion shape	complex	C–H...A	C–H	H...A	C...A	∠C–H–A
tetrahedral	[Fe ₂ L ₃ (BF ₄)](BF ₄) ₆ (1)	C10–H10...F2	0.95	2.49	2.998	112.9
	[Fe ₂ L ₃ (ClO ₄)](ClO ₄) ₆ (2)	C10–H10...O2	0.95	2.52	3.009	112.7
	[Fe ₂ L ₃ (SO ₄) ₂](SO ₄) ₅ (3)	C10–H10...O2	0.95	2.43	2.935	113.7
spherical	[Fe ₂ L ₃ (Br)](BPh ₄) ₆ (4)	C14 ⁺ –H14...Br	0.95	2.66	3.602	170.7
trigonal planar	[Cu ₂ L ₃ (NO ₃)](NO ₃) ₆ (6)	C14 ⁺ –H14...O1	0.95	1.35	2.223	150.6

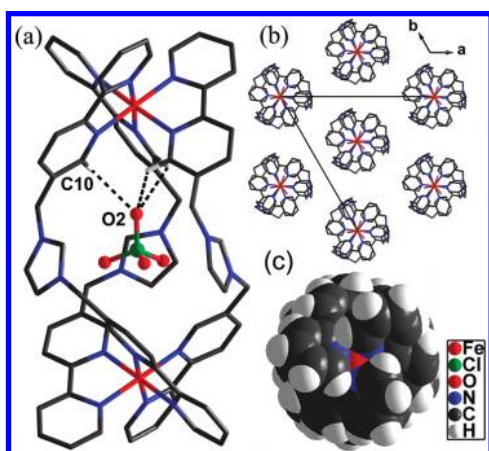


Figure 3. (a) Molecular structure of the cationic unit ($\Delta\Delta$)-[Fe₂L₃OClO₄]⁶⁺ of **2**. Noninteracting H atoms and external counteranions were omitted for clarity. (b) Packing diagram. (c) Space-filling depiction.

10.5 Å, which is comparable with that in the tetrafluoroborate complex **1**.

[Fe₂L₃(SO₄)₂](SO₄)₅·3CH₃CN (**3**). Another isomorphous iron(II) complex **3** was obtained in a similar way. In complex **3**, the “pseudo-C”-shaped ligands form a triple-stranded mesocate [Fe₂L₃SO₄]⁵⁺. There are two independent iron(II) complex units, five SO₄²⁻ counterions, and three acetonitrile molecules in the crystal structure (Figure 4), as demonstrated by

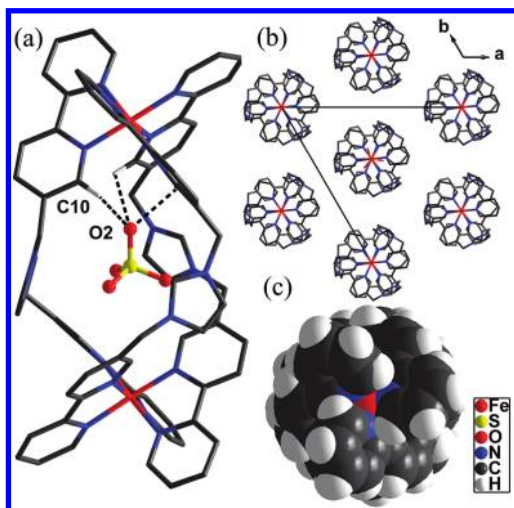


Figure 4. (a) Molecular structure of one of the independent cationic units ($\Delta\Delta$)-[Fe₂L₃SO₄]⁵⁺ of **3**. Noninteracting H atoms and external counteranions were omitted for clarity. (b) Packing diagram. (c) Space-filling depiction.

elemental analysis and X-ray diffraction. One of the O atoms (O2) of the encapsulated SO₄²⁻ ion sits at a C₃ axis and forms

three C_{py}–H...O hydrogen bonds as in the cases of **1** and **2** [C10...O2, 2.967(3) Å; Table 1]. There are also strong electrostatic interactions between the central anion and the cationic cage due to the short distances from the anion to the imidazolium rings [C14...O1, 3.100(5) Å]. The Fe...Fe separation is ca. 10.6 Å.

[Fe₂L₃Br](BPh₄)₆·3CH₃CN (**4**). The structure of complex **4** consists of a cationic cage capsule [Fe₂L₃Br]⁶⁺ and six BPh₄⁻ counterions, as well as three acetonitrile molecules (Figure 5).

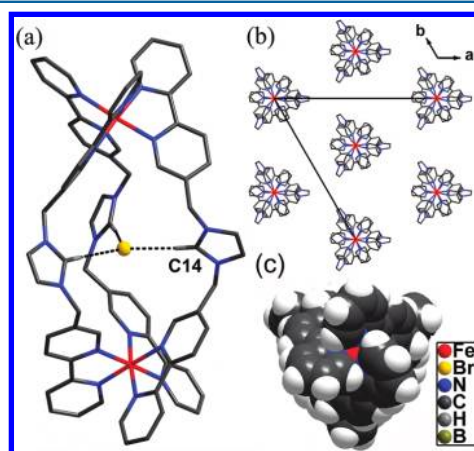


Figure 5. (a) Molecular structure of the cationic unit ($\Delta\Delta$)-[Fe₂L₃Br]⁶⁺ of **4**. Noninteracting H atoms and external counteranions were omitted for clarity. (b) Packing diagram. (c) Space-filling depiction.

Three ligands wrap around two Fe^{II} ions to yield a triple-stranded structure with a highly charged central cage. Instead of forming a mesocate like **1–3**, the ligands adopt a “pseudo-S” shape and lead to the same configuration at the two Fe^{II} centers. Therefore, a helicate was obtained with an approach angle of 52.5°.^{6f} Very interestingly, the carbenic C atoms of the bridging imidazolium groups are oriented toward the center of the cage. A relatively small Br⁻ anion rather than the large BPh₄⁻ is efficiently encapsulated in the center of the cage via three C–H...Br⁻ ionic hydrogen bonds [C14...Br, 3.602(3) Å] from the imidazolium groups (Table 1). This is in contrast to the mesocates **1–3** discussed above, in which the imidazolium CH⁺ donors deviate from the equatorial plane of the Fe₂L₃ complex and cannot form effective C–H...X hydrogen bonds with the anion.

The dimensions of the cage are defined by the Fe...Fe (ca. 11.8 Å) and imidazolium...imidazolium (ca. 5.7 Å between centroids) separations. Compared to the tetrahedral anion-encapsulating complexes **1–3**, the Fe...Fe distance is slightly longer, while the “available volume” of the cavity is smaller (Figure S5 in the Supporting Information) because the imidazolium CH⁺ donors are now oriented inward toward the center to hydrogen-bond the guest anion. A packing diagram (Figure 5b)

of **4** indicates that every one cage is surrounded by six such cages via interaction with external BPh_4^- ions and CH_3CN solvents. Notably, the structure is chiral (with the space group $R3$), and all of the $[\text{Fe}_2\text{L}_3]$ molecules are the same P helix, with the Δ configuration about both metal centers. Several crystals have been tested, and all of them displayed the same chirality. The results indicate that only one of the helical enantiomers has crystallized from the solution. We have also measured the circular dichroism spectrum of a solution of the crystals, but no optical activity was observed. Thus, spontaneous resolution may have occurred during crystallization of the triple helicate, but the complex racemized rapidly in solution [9:1 (v/v) $\text{CH}_3\text{CN}/\text{H}_2\text{O}$] at room temperature.

$[\text{Cu}_2\text{L}_3\text{O}(\text{NO}_3)](\text{NO}_3)_6$ (**6**). The copper(II) nitrate complex **6** shows a structure similar to that of the iron(II) bromide analogue **4**, in which one nitrate anion is encapsulated within the central cage of the complex (Figure 6). The three “S”-shaped

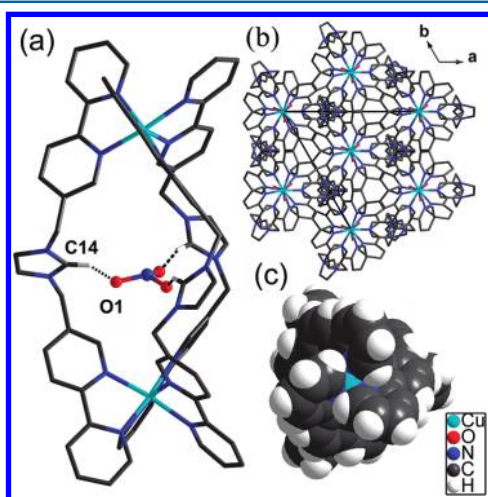


Figure 6. (a) Molecular structure of the cationic unit $(\Delta\Delta)$ - $[\text{Cu}_2\text{L}_3\text{O}(\text{NO}_3)]^{6+}$ of **6**. Noninteracting H atoms and external counteranions were omitted for clarity. (b) Packing diagram. (c) Space-filling depiction.

ligands also wrap the two Cu^{II} centers to construct a triple-stranded helicate with an approach angle of 55.6° ,^{6f} which is slightly larger than that in complex **4**. Like the bromide-including complex **4**, this helicate is also chiral in the solid state, showing only the P configuration. Each Cu^{II} ion is coordinated by three bpy units through C_3 symmetry in an octahedral arrangement without apparent Jahn–Teller distortion, and all six Cu–N bond distances are essentially identical. The absence of Jahn–Teller distortion in other copper(II) complexes has also been reported.^{16g,19} The N atom of the encapsulated nitrate anion sits at the crystallographic C_3 axis, and the three C_3 -related O atoms form three charge-assisted C–H \cdots O $^-$ [C14 \cdots O1, 2.223(3) Å] hydrogen bonds with the bridging imidazolium units, which also point to the center of the cage as in **4**. Notably, the trapped nitrate ion is not planar. The N atom is slightly out of the plane defined by the three O atoms, with the sum of the O–N–O angles being 350.7° . This distortion is apparently caused by the spatial crowding of the nitrate ion, which has to be located on the equatorial plane of the complex cage to form hydrogen bonds with the CH donors of the imidazolium groups (Figure 6a). It is noticeable that the C \cdots O distance (2.223 Å) of this C–H \cdots O hydrogen bond is very short (Table 1). Each complex is also surrounded by six neighbors via interactions with

external NO_3^- ions (Figure 6b). The size of the cage is identified by ca. 11.7 Å (Cu \cdots Cu distance). This longer metal \cdots metal separation in the helicates **4** and **6** than in the mesocates **1–3** agrees with the results observed by Raymond et al. that the two vertex metals of a guest-free helicate with a narrow cavity is longer than that of a water-encapsulating mesocate with a broad cavity (Figures S5 and S6 in the Supporting Information).⁷

NMR Studies. In the current work, as discussed above, the ligand conformation and anion-binding mode in the helicates and mesocates are significantly different, which can lead to distinct NMR signals and thus should allow for the evaluation of their structures in solution. Two complexes, **1** and **5**, were used as the representatives of mesocate and helicate, respectively. The complexes were examined by NMR experiments performed in $\text{CD}_3\text{CN}/\text{H}_2\text{O}$ (8:1, v/v) at room temperature, and both of the ^1H and ^{13}C NMR studies revealed the characteristics of the two complexes. In the ^1H NMR spectra, the two structures displayed dramatically different features for all of the protons, including the bpy units, the NCHCHN protons of the imidazolium, the carbenic CH^+ , and the CH_2 linkers. In the helicate structure **5**, a distinct downfield shift ($\Delta\delta = 1.18$ ppm) of the carbenic CH^+ H atom was observed, indicating direct interactions with the central anion via strong hydrogen bonding, yet a well-distinguishable upfield shift ($\Delta\delta = -0.45$ ppm) of this proton in the mesocate **1** resulted because of the shielding effects of the nearby aryl rings. For the protons of NCHCHN in the central imidazolium groups, only one signal was observed in the “S”-shaped ligand of the helicate, while the mesocate displayed two sets of singlets at 6.86 and 6.96 ppm. Also, significant changes occurred for the signals of the CH_2 linkers, which appeared as a singlet in the free ligand but appeared two groups of peaks in the helicate **5** and further split into four sets of peaks in the mesocate **1** (Figure 7a).

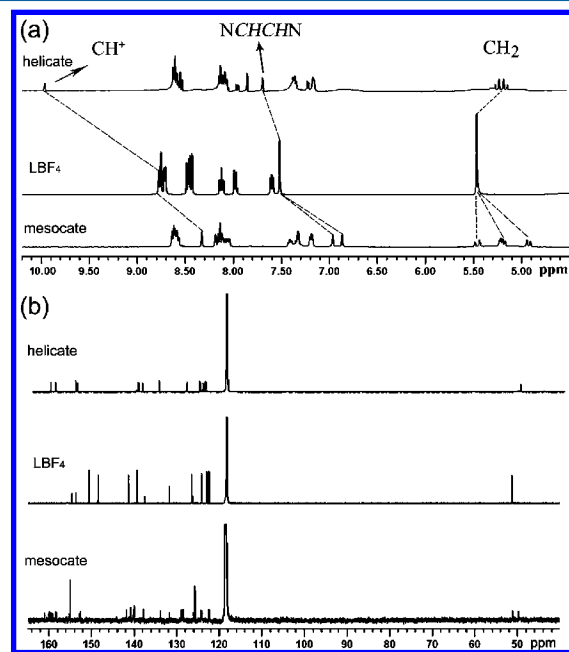


Figure 7. ^1H and ^{13}C NMR spectra of the mesocate **1** and helicate **5** in $\text{CD}_3\text{CN}/\text{H}_2\text{O}$ (8:1, v/v) at room temperature.

These results clearly reflected the structural character of the mesocate and helicate and can be well explained by the

different symmetries of the two enantiomers caused by the conformational change of the ligand upon anion binding. In the mesocate, the encapsulated tetrahedral anion sits at a C_3 axis, with one terminal atom (F or O) pointing to one $[\text{Fe}(\text{bpy})_3]^{2+}$ head (Figure 2, upper part) and the other three F or O atoms to the other $[\text{Fe}(\text{bpy})_3]^{2+}$ head (Figure 1, lower part). In contrast, in the helicate, the NO_3^- or Br^- anion is located on the equatorial plane and gives a symmetric structure. As a result, the mesocate displays more signals in the ^1H NMR spectrum. The results also revealed that the mesocate or helicate structure should be persistent in the solution. Moreover, because the Py 6-CH of one side forms weak $\text{C}\cdots\text{H}\cdots\text{X}$ hydrogen bonds with the anion in the mesocate, the bpy protons in the two sides should appear at different positions. However, these protons are highly overlapped and cannot be well distinguished in the two cases.

The ^{13}C NMR spectra are in good agreement with the ^1H NMR results and further confirmed the different environments of the protons in the two cases. The mesocate displayed 25 signals, with the NCHCHN moiety showing two signals at 151.3 and 140.5 ppm and the CH_2 group splitting into two peaks at 50.9 and 49.6 ppm, respectively. Notably, the bpy units in the two head groups of the mesocate display different chemical shifts in the case of the ^{13}C NMR spectrum. Accordingly, the more symmetric helicate shows 13 signals (half of the total C atoms). This is in accordance with their structures in the solid state (Figure S4 in the Supporting Information). In addition, some protons showed upfield shifts compared to the free ligand, suggesting that they now probably lie in the shielding region upon formation of the metal complexes. The ^{19}F NMR spectrum of **1** recorded in D_2O at high concentration (10^{-4} M) also provided evidence for the asymmetric structure of the meso species. The free LBF_4 ligand displayed two very closely spaced peaks at ca. -150 ppm (-150.5 and -150.4 ppm) in the ^{19}F NMR spectrum corresponding to the two isotopes of boron in their natural abundance (Figure S7 in the Supporting Information).²⁰ Upon formation of the $[\text{Fe}_2\text{L}_3\text{C}(\text{BF}_4)](\text{BF}_4)_6$ complex, there were four separated signals. The two upfield signals ($-150.0/-150.1$ and $-147.7/-147.8$ ppm) are assigned to the six external BF_4^- counterions, which are under slightly different environments. The slightly downfield-shifted (ca. 2 ppm) signals may be attributed to the anions that are close to the imidazolium CH^+ groups and have weak interactions with them, and the other peaks, which are almost unchanged compared to the ligand LBF_4 , are attributed to those apart from the CH^+ groups and thus can be viewed as free anions. The two signals appearing at the more downfield region ($-143.4/-143.5$ and -129.7 ppm, respectively) can be attributed to the encapsulated BF_4^- ion. The signal of the F atom sitting at the C_3 axis and those of the other three F atoms show a proper integral ratio of ca. 1:3.

Formation of Helicates versus Mesocates. Since Albrecht and co-workers first synthesized a triple-stranded mesocate in 1995,^{1b} chemists have been attempting to control the formation of helicates versus mesocates. On the basis of the self-assembly of a series of dicatechol ligands, Albrecht and co-workers^{3b,6d} proposed an empirical *odd-even* rule. It was suggested that tuning the length of the alkyl linker can lead to the “S” (with an even number of C atoms of the alkyl linker) or “C” (with an odd number of C atoms) conformation of the ligand and thus facilitates the formation of a helicate or a mesocate, respectively. In addition, theoretically, the homochiral helicate consistently shows a lower total energy and is preferred

generally.^{3d} Recently, Dolphin and co-workers^{5b} successfully synthesized and isolated both triple-stranded helicates and mesocates from the same reaction, employing an α -free, β,β' -linked bis(dipyromethene) with a methylene bridge. They found that the ligand can take either a pseudo-S or a pseudo-C conformation through bond rotation owing to the ready transition between the two conformers under the reaction conditions and result in both structures.

Considering the minimum energy of the complex and the optimal “S” conformation taken by the free ligand LBr (Figure 1) as mentioned above, the helicate structure should be favored for the $[\text{M}_2\text{L}_3]$ assemblies reported in this work. Interestingly, it was found that anions of different sizes and shapes were brought into this system, and the relatively larger tetrahedral anions like BF_4^- led to the formation of meso complexes (Figures 2–4), whereas the smaller spherical Br^- and trigonal-planar NO_3^- favored the helicates (Figures 5 and 6) by spontaneous resolution during crystallization. These results imply that the anions may have templated the selective formation of the mesocates or helicates. In order to accommodate the anion in the central cage, which has a great contribution to stabilization of the final $[\text{M}_2\text{L}_3]$ structure, the complex has to adjust itself to the size of the guest by stretching or compression, accompanied by the conformational change of the ligand, to achieve the optimum state. As depicted in Figures 2–4, for the large tetrahedral anions, the CH^+ vector of the bridging imidazolium group was twisted to the tangent direction to release enough inner space. This orientation then forced the strands to be parallel to the C_3 axis and adopt a “pseudo-C” shape to avoid steric repulsion of the bpy and imidazolium rings, thus leading to the meso configuration. In comparison, in the presence of relatively small anions, the CH^+ groups rotated and oriented toward the center cage and formed efficient $\text{CH}^+\cdots\text{X}^-$ ionic hydrogen bonds. The strands took a “pseudo-S” shape, which reduced the steric repulsion to a large extent, and a helicate configuration was constructed (Figure 8). Besides the effect of the ligand

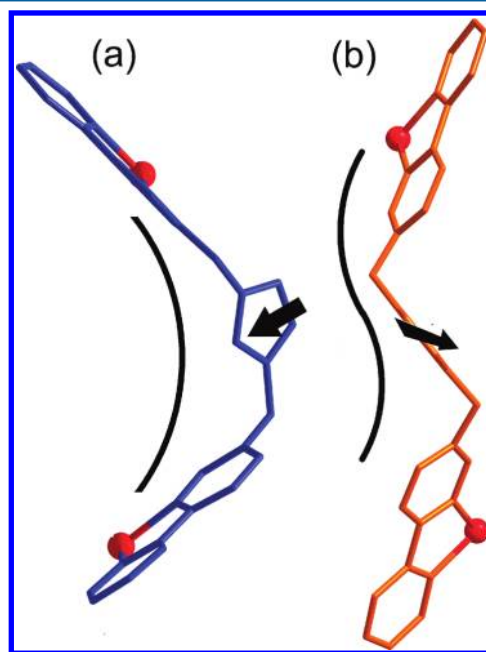


Figure 8. View of the “pseudo-C” conformer of the ligand in the mesocate complexes (a) and the “pseudo-S” conformer in the helicate complexes (b).

conformation, the coordination and hydrogen-bonding ability of the anions may also count for distinction of the two isomers. The mesocates were formed when the anions do not hydrogen-bond to the imidazolium cations, while the helicates were obtained with the halides or nitrate, which form such hydrogen bonds.

For the purpose of achieving stable mesocates, many efforts have been devoted recently, such as engrafting *R*- and *S*-chiral groups in proximity to the chelating units or designing the zigzag conformation of alkyl spacers containing an *odd* number of methylene units employed.^{3a,b} Here we realized the effective stabilization of the mesocate structure and spontaneous resolution of mesocates and helicates controlled by the size of the anions.

CONCLUSIONS

We have successfully synthesized a series of highly charged, dinuclear triple-stranded cage-like $[M_2L_3]^{7+}$ complexes by employing an imidazolium-bridged bis(2,2'-bipyridine) ligand (L) and a Fe^{II} or Cu^{II} ion. Interestingly, the complex can accommodate an anion in the cage, and the size and/or shape of the encapsulated anion is the key factor that determines the stereochemistry of the product. In the presence of the larger tetrahedral anions such as BF₄⁻, SO₄²⁻, and ClO₄⁻, the meso complexes are favored. In contrast, the smaller trigonal-planar (NO₃⁻) or spherical (Br⁻) anions lead to helicates. Moreover, spontaneous resolution of the *P* helices occurred during crystallization of the helicates 4 and 6. The conformational change of the ligand upon encapsulation of the anion may be responsible for the anion-dependent formation of the helicates versus mesocates.

EXPERIMENTAL SECTION

General Procedures. ¹H, ¹³C, and ¹⁹F NMR spectra were recorded on a Mercury plus-400 spectrometer at 400, 100, and 375.99 MHz, using tetramethylsilane and NaBF₄ as internal standards, respectively, FT-IR spectra were measured by a Nicolet AVATAR 360 FT-IR spectrometer as KBr disks. Elemental analyses were performed on a VarioEL from Elementaranalysesysteme GmbH. Melting points were detected on an X-4 Digital Vision MP Instrument. Powder X-ray diffraction patterns were obtained with a D/max RB diffractometer using Mo K α radiation. ESI-MS measurements were carried out using a Waters ZQ4000 spectrometer in water and a Bruker MicrOTOF-Q in ESI positive-ion mode.

5-Methyl-2,2'-bipyridine was prepared by the traditional Kröhnke procedure from 2-acetylpyridine and methacrolein according to the literature procedures.²¹ 5-(Bromomethyl)-2,2'-bipyridine was prepared from 5-methyl-2,2'-bipyridine by reaction with an excess of *N*-bromosuccinimide with azobis(isobutyronitrile) as the initiator under an N₂ atmosphere, as reported in the literature.²² The target ligand was prepared using modified procedures.¹⁷

Synthesis of *N,N'*-Bis[5-(2,2'-bipyridyl)methyl]imidazolium Bromide (LBr). 5-(Bromomethyl)-2,2'-bipyridine (1.94 g, 10.0 mmol) and imidazole (1.00 g, 4.00 mmol) were heated under reflux in dry acetonitrile (50 mL) for 48 h. The reaction mixture was cooled to room temperature and the solvent removed in vacuo. The addition of dichloromethane to the residue gave rise to the formation of a yellow precipitate, which was collected by filtration and recrystallized in water to yield a white powder (1.18 g, 51%). Mp: 209–212 °C. ¹H NMR (DMSO-*d*₆, 400 MHz): δ 9.52 (s, 1H, CH⁺), 8.82 (br s, 2H, H6'), 8.71 (d, *J* = 4.0 Hz, 2H, H6), 8.39–8.46 (m, 4H, overlapping H3 and H3'), 7.98–8.06 (m, 4H, overlapping H4' and H4), 7.96 (s, 2H, NCHCHN), 7.48–7.51 (m, 2H, H5'), 5.59 (s, 4H, CH₂). ESI-MS: *m/z* 405.2 ([M – Br]⁺) (calcd 405.2).

Crystal data for LBr: C₂₅H₂₁BrN₆ (485.39), colorless block, crystal system monoclinic, space group P2(1)/c, *a* = 8.8357(11) Å,

b = 13.0305(17) Å, *c* = 19.233(2) Å, β = 101.492(2)°, *V* = 101.492(2) Å³, *T* = 153(2) K, *Z* = 4, *D*_c = 1.486 g cm⁻³, *F*₀₀₀ = 992, μ = 1.92 mm⁻¹, 13 887 reflections collected, 3817 unique (*R*_{int} = 0.0289), 3037 observed [*I* > 2 σ (*I*)]; final *R*1 = 0.041, *wR*2 = 0.12 [*I* > 2 σ (*I*)].

Synthesis of Complexes [Fe₂L₃(BF₄)](BF₄)₆ (1), [Fe₂L₃(ClO₄)](ClO₄)₆ (2), [Fe₂L₃(SO₄)₂(SO₄)₅ (3), and [Fe₂L₃(Br)](BPh₄)₆ (4). To a stirred suspension of LBr (100 mg, 0.206 mmol) in 2 mL of water was added dropwise an aqueous solution of FeBr₂·6H₂O (44.5 mg, 0.137 mmol). An immediate color change from colorless to red marked the complex formation. The resulting deep-red solution was stirred for 30 min at room temperature and then treated with a 10-fold excess of the aqueous solution of NaX [X = BF₄⁻ (1), ClO₄⁻ (2), SO₄²⁻ (3), and BPh₄⁻ (4)]. A deep-red precipitate was filtered off, washed with EtOH and ether, and dried.

[Fe₂L₃(BF₄)](BF₄)₆ (1). Yield: 118 mg, 89%. Anal. Calcd for [Fe₂L₃(BF₄)](BF₄)₆·4H₂O (C₇₅H₇₁B₇F₂₈Fe₂N₁₈O₄): C, 44.87; H, 3.56; N, 12.56. Found: C, 44.80; H, 3.42; N, 12.86. FT-IR (KBr, ν /cm⁻¹): 3164w, 3115w, 1612m, 1563m, 1474m, 1440m, 1405w, 1165m, 1064s (br, BF₄⁻), 846w, 762m, 521w. ¹H NMR [8:1 (v/v) CD₃CN/H₂O, 400 MHz]: δ 8.64–8.56 (m, 4H, bpy-3' and -3), 8.32 (s, 1H, CH⁺), 8.18–8.04 (m, 6H, bpy-4, -4', and 6'), 7.42–7.32 (m, 2H, bpy-5'), 7.20–7.17 (m, 2H, bpy-6'), 6.96 (s, 1H, NCHCHN), 6.86 (s, 1H, NCHCHN), 5.46 (d, *J* = 16 Hz, 1H, CH₂), 5.23–5.17 (m, 2H, CH₂), 4.92 (d, *J* = 16 Hz, 1H, CH₂). ¹³C NMR [8:1 (v/v) CD₃CN/H₂O, 100 MHz]: δ 160.8 (CH⁺), 159.8, 159.7, 159.2, 158.9, 158.0, 154.8, 154.7, 152.4 (NCHCHN), 141.5 (NCHCHN), 140.6, 139.9, 139.7, 137.5, 133.5, 131.4, 128.6, 128.2, 125.7, 125.4, 124.0, 123.8, 122.2, 50.9 (CH₂), 49.6 (CH₂). ESI-MS: *m/z* 881.2 ([Fe₂L₃(BF₄)₅]²⁺).

[Fe₂L₃(ClO₄)](ClO₄)₆ (2). Yield: 125 mg, 90%. Anal. Calcd for [Fe₂L₃(ClO₄)](ClO₄)₆ (C₇₅H₆₃Cl₇Fe₂N₁₈O₂₈): C, 44.50; H, 3.14; N, 12.45. Found: C, 44.86; H, 3.10; N, 12.70. FT-IR (KBr, ν /cm⁻¹): 3110w, 3094w, 1608w, 1560w, 1464m, 1438m, 1162m, 1083s (br, ClO₄⁻), 753m, 615s. ¹H NMR [8:1 (v/v) CD₃CN/H₂O, 400 MHz, ppm]: δ 8.61–8.57 (m, 2H, bpy-3'), 8.01 (s, 1H, CH⁺), 8.25–8.23 (m, 2H, bpy-3), 8.14–8.10 (m, 2H, bpy-4), 7.88 (s, 2H, bpy-6), 7.57–7.54 (m, 2H, bpy-4'), 7.97 (s, 1H, NCHCHN), 7.87 (s, 1H, NCHCHN), 7.36 (dd, *J* = 4.8 and 8.0 Hz, 2H, bpy-6'), 7.26 (dd, *J* = 4.8 and 8.0 Hz, 2H, bpy-5'), 5.53 (s, 1H, CH₂), 5.34–5.25 (m, 2H, CH₂), 5.12 (s, 1H, CH₂). ¹³C NMR [8:1 (v/v) CD₃CN/H₂O, 100 MHz]: δ 163.4 (CH⁺), 158.3, 158.2, 153.7, 148.2 (NCHCHN), 147.7 (NCHCHN), 141.7, 141.6, 138.7, 137.4, 137.2, 127.6, 127.5, 127.4, 127.3, 127.2, 124.4, 124.3, 123.7, 123.6, 123.1, 118.1, 118.0, 49.2 (CH₂), 49.1 (CH₂). ESI-MS: *m/z* 912.1 ([Fe₂L₃(ClO₄)₅]²⁺).

[Fe₂L₃(SO₄)₂(SO₄)₅ (3). Yield: 102 mg, 89%. Anal. Calcd for [Fe₂L₃(SO₄)₂(SO₄)₅ (C₁₅₀H₁₂₆Fe₄N₃₆O₂₈S₇): C, 54.12; H, 3.82; N, 15.15. Found: C, 54.46; H, 3.48; N, 15.12. FT-IR (KBr, ν /cm⁻¹): 3045w, 2974w, 1629m, 1604m, 1559m, 1468m, 1438m, 1412m, 1156m, 1115m (SO₄²⁻), 767m. ¹H NMR [4:1 (v/v) CD₃CN/H₂O, 400 MHz, ppm]: δ 8.97 (s, 1H, CH⁺), 8.64–8.62 (m, 4H, bpy-3' and -3), 8.15–8.08 (m, 6H, bpy-4, -4', and -6), 7.42–7.32 (m, 2H, bpy-5'), 7.22–7.21 (m, 2H, bpy-6'), 7.88 (s, 1H, NCHCHN), 7.72 (s, 1H, NCHCHN), 5.45 (s, 1H, CH₂), 5.32–5.16 (m, 2H, CH₂), 5.05 (s, 1H, CH₂). ¹³C NMR and the M₂L₃ species in the MS spectrum could not be accessed because of the poor solubility of complex 3 (decomposition may occur when the concentration is too low).

[Fe₂L₃(Br)](BPh₄)₆ (4). Yield: 112 mg, 88%. Anal. Calcd for [Fe₂L₃(Br)](BPh₄)₆ (C₂₁₉H₁₈₃B₆BrFe₂N₁₈): C, 79.15; H, 5.55; N, 7.59. Found: C, 78.71; H, 5.22; N, 7.66. FT-IR (KBr, ν /cm⁻¹): 3050w, 2958w, 2923w, 1661m, 1599m, 1558m, 1466m, 1436m, 1400m, 1242m, 1155m, 1088m, 736m, 700m, 603m. ¹H NMR [4:1 (v/v) CD₃CN/H₂O, 400 MHz, ppm]: δ 10.3 (s, 1H, CH⁺), 8.61–8.57 (m, 2H, bpy-3'), 8.45–8.36 (m, 2H, bpy-3), 8.11–8.04 (m, 2H, bpy-4'), 7.86 (s, 2H, NCHCHN), 7.74 (m, 4H, BPh₄), 7.63–7.58 (m, 2H, bpy-4), 7.45–7.42 (m, 2H, bpy-6), 7.36–7.32 (m, 2H, bpy-5'), 7.23 (s, 8H, BPh₄), 7.19–7.15 (m, 2H, bpy 6'), 6.92 (s, 8H, BPh₄), 4.68–4.61 (m, 4H, CH₂). ¹³C NMR [8:1 (v/v) CD₃CN/H₂O, 100 MHz]: δ 164.2 (CH⁺), 163.7, 163.2, 162.7, 156.5 (NCHCHN), 153.5, 135.3, 129.2, 128.6, 127.3, 127.1, 126.5, 125.4, 121.6, 119.2, 114.9, 35.7 (CH₂). ESI-MS: *m/z* 1342.5 ([Fe₂L₃(BPh₄)₄Br]²⁺).

Synthesis of $\text{Fe}_2\text{L}_3(\text{NO}_3)_2\text{Br}_6$ (5). To a stirred suspension of LBr (100 mg, 0.206 mmol) in 2 mL of water was added dropwise a MeOH solution of $\text{Fe}(\text{NO}_3)_3 \cdot 9\text{H}_2\text{O}$ (55.4 mg, 0.137 mmol) in the presence of excess iron powder. An immediate color change from colorless to red marked the complex formation. The resulting deep-red mixture was stirred for 30 min at room temperature and then filtered through Celite. The filtrate was reduced to 4 mL. A deep-purple precipitate was obtained through the slow diffusion of ether into the solution of the product at room temperature. Yield: 92 mg, 70%. Anal. Calcd for $[\text{Fe}_2\text{L}_3(\text{NO}_3)]\text{Br}_6 \cdot 2\text{H}_2\text{O}$ ($\text{C}_{75}\text{H}_{67}\text{Fe}_2\text{Br}_6\text{N}_{19}\text{O}_5$): C, 50.22; H, 3.76; N, 14.84. Found: C, 50.47; H, 4.05; N, 14.99. FT-IR (KBr, ν/cm^{-1}): 3050w, 2853w, 1637w, 1606w, 1561m, 1468m, 1438m, 1383s (NO_3^-), 1161m, 766m. ^1H NMR [8:1 (v/v) $\text{CD}_3\text{CN}/\text{H}_2\text{O}$, 400 MHz]: δ 9.95 (s, 1H, CH^+), 8.62–8.52 (m, 4H, bpy-3' and -3), 8.15–8.06 (m, 2H, bpy-4'), 7.96–7.94 (dd, $J = 1.6$ and 8.0 Hz, 2H, bpy-4), 7.85 (d, $J = 1.6$ Hz, 2H, bpy-6), 7.69 (s, 2H, NCHCHN), 7.37–7.34 (m, 2H, bpy-5'), 7.22–7.15 (dd, $J = 1.6$ and 8.0 Hz, 2H, bpy-6'), 5.27–5.14 (m, 4H, CH_2). ^{13}C NMR [8:1 (v/v) $\text{CD}_3\text{CN}/\text{H}_2\text{O}$, 100 MHz]: δ 159.5 (CH^+), 158.4, 153.7, 153.3 (NCHCHN), 139.0, 138.8, 138.0, 134.1, 127.6, 124.5, 123.9, 123.3, 49.2 (CH_2). ESI-MS: m/z 836.6 ($[\text{Fe}_2\text{L}_3(\text{NO}_3)_3\text{Br}_2]^{2+}$), 846.1 ($[\text{Fe}_2\text{L}_3(\text{NO}_3)_2\text{Br}_3]^{2+}$), 854.5 ($[\text{Fe}_2\text{L}_3(\text{NO}_3)\text{Br}_4]^{2+}$).

Synthesis of $[\text{Cu}_2\text{L}_3(\text{NO}_3)](\text{NO}_3)_6$ (6). To a stirred suspension of LBr (100 mg, 0.206 mmol) in 2 mL of water was added dropwise an aqueous solution of $\text{Cu}(\text{NO}_3)_2 \cdot 3\text{H}_2\text{O}$ (33.2 mg, 0.137 mmol). An immediate color change from colorless to blue marked the complex formation. The mixture was stirred for 30 min at room temperature. A blue precipitate was filtered off, washed with EtOH and ether, and dried. Blue crystals were obtained by the slow diffusion of ether into a CH_3CN solution of the product at room temperature. Yield: 112 mg, 88%. Anal. Calcd for $[\text{Cu}_2\text{L}_3(\text{NO}_3)](\text{NO}_3)_6$ ($\text{C}_{75}\text{H}_{63}\text{Cu}_2\text{N}_{25}\text{O}_{21}$): C, 50.68; H, 3.57; N, 19.70. Found: C, 50.74; H, 3.87; N, 19.31. FT-IR (KBr, ν/cm^{-1}): 3050w, 2924w, 1605w, 1563w, 1503w, 1473w, 1440w, 1383s (NO_3^-), 1162w, 1052w, 759w, 670w. ESI-MS: m/z 1328.1 ($[\text{Cu}_2\text{L}_2(\text{NO}_3)_5(\text{CH}_3\text{CN})_2]^+$); only the M_2L_2 species can be detected).

X-ray Crystal Structure Determination. X-ray diffraction data for the complexes were collected on a Bruker SMART APEX II diffractometer at 150 K with graphite-monochromated Mo $K\alpha$ radiation ($\lambda = 0.71073$ Å). Multiscan corrections were applied using SADABS.²³ Structure solutions and refinements were performed with the SHELX-97 package.²⁴ All non-H atoms were refined anisotropically by full-matrix least squares on F^2 . H atoms bonded to C and N atoms were included in idealized geometric positions, with thermal parameters equivalent to 1.2 times those of the atom to which they were attached. The $wR2$ value for complex 3 is quite high, which may be due to the presence of a considerable amount of weak diffraction. The NO_3^- anion in complex 6 is not perfectly planar because of the small space of the cage in the helicate as discussed above.

Crystal data for 1: $\text{C}_{81}\text{H}_{72}\text{B}_7\text{F}_{28}\text{Fe}_2\text{N}_{21}$ (2058.97), red block, crystal system rhombohedral, space group $R3$, $a = 20.542(2)$ Å, $b = 20.542(2)$ Å, $c = 17.928(2)$ Å, $\alpha = \beta = 90^\circ$, $\gamma = 120^\circ$, $V = 6551.6(13)$ Å³, $T = 153(2)$ K, $Z = 3$, $D_c = 1.566$ g cm⁻³, $F_{000} = 3132$, $\mu = 0.45$ mm⁻¹, 15 403 reflections collected, 5944 unique ($R_{\text{int}} = 0.029$), 5269 observed [$I > 2\sigma(I)$]; final $R1 = 0.046$, $wR2 = 0.14$ [$I > 2\sigma(I)$].

Crystal data for 2: $\text{C}_{81}\text{H}_{72}\text{Cl}_7\text{Fe}_2\text{N}_{21}\text{O}_{28}$ (2147.45), red block, crystal system rhombohedral, space group $R3$, $a = 20.675(4)$ Å, $b = 20.675(4)$ Å, $c = 17.902(4)$ Å, $\alpha = \beta = 90^\circ$, $\gamma = 120^\circ$, $V = 6627(13)$ Å³, $T = 153(2)$ K, $Z = 3$, $D_c = 1.614$ g cm⁻³, $F_{000} = 3132$, $\mu = 0.64$ mm⁻¹, 13 777 reflections collected, 5165 unique ($R_{\text{int}} = 0.056$), 3967 observed [$I > 2\sigma(I)$]; final $R1 = 0.059$, $wR2 = 0.15$ [$I > 2\sigma(I)$].

Crystal data for 3: $\text{C}_{81}\text{H}_{72}\text{Fe}_2\text{N}_{21}\text{O}_{22}\text{S}_7$ (2027.72), red block, crystal system rhombohedral, space group $R3$, $a = 20.526(6)$ Å, $b = 20.526(6)$ Å, $c = 17.924(5)$ Å, $\alpha = \beta = 90^\circ$, $\gamma = 120^\circ$, $V = 6540(3)$ Å³, $T = 153(2)$ K, $Z = 3$, $D_c = 1.545$ g cm⁻³, $F_{000} = 3135$, $\mu = 0.59$ mm⁻¹, 12 427 reflections collected, 6496 unique ($R_{\text{int}} = 0.056$), 4629 observed [$I > 2\sigma(I)$]; final $R1 = 0.085$, $wR2 = 0.246$ [$I > 2\sigma(I)$].

Crystal data for 4: $\text{C}_{231}\text{H}_{201}\text{B}_6\text{BrFe}_2\text{N}_{24}$ (3569.63), red block, crystal system rhombohedral, space group $R3$, $a = 26.490(5)$ Å, $b = 26.490(5)$ Å, $c = 23.483(4)$ Å, $\alpha = \beta = 90^\circ$, $\gamma = 120^\circ$, $V = 14271(4)$ Å³, $T = 153(2)$ K, $Z = 3$, $D_c = 1.246$ g cm⁻³, $F_{000} = 5616$, $\mu = 0.43$ mm⁻¹,

31011 reflections collected, 11 121 unique ($R_{\text{int}} = 0.073$), 7049 observed [$I > 2\sigma(I)$]; final $R1 = 0.055$, $wR2 = 0.16$ [$I > 2\sigma(I)$].

Crystal data for 6: $\text{C}_{75}\text{H}_{63}\text{Cu}_2\text{N}_{21}\text{O}_{11}$ (1561.57), blue block, crystal system rhombohedral, space group $R3$, $a = 13.563(12)$ Å, $b = 13.563(12)$ Å, $c = 42.74(4)$ Å, $\alpha = \beta = 90^\circ$, $\gamma = 120^\circ$, $V = 6809(10)$ Å³, $T = 153(2)$ K, $Z = 3$, $D_c = 1.142$ g cm⁻³, $F_{000} = 2418$, $\mu = 0.53$ mm⁻¹, 15 111 reflections collected, 5259 unique ($R_{\text{int}} = 0.049$), 2903 observed [$I > 2\sigma(I)$]; final $R1 = 0.055$, $wR2 = 0.15$ [$I > 2\sigma(I)$].

■ ASSOCIATED CONTENT

● Supporting Information

Characterization of LBr and the complexes and detailed information of the X-ray crystal structure analysis of compounds 1–4 and 6 (CIF files). This material is available free of charge via the Internet at <http://pubs.acs.org>.

■ AUTHOR INFORMATION

Corresponding Author

*E-mail: wubiao@lzb.ac.cn.

■ ACKNOWLEDGMENTS

This work was supported by the National Natural Science Foundation of China (Grant 20872149). The authors thank Dr. Deliang Long, The University of Glasgow, for help with MS. J.S.M. and L.C. thank WestCHEM and the EPSRC for funding.

■ REFERENCES

- (a) Lindsey, J. S. *New J. Chem.* **1991**, *15*, 153–180. (b) Carrano, C. J.; Raymond, K. N. *J. Am. Chem. Soc.* **1978**, *100*, 5371–5378. (c) Elliott, C. M.; Derr, D. L.; Ferrere, S.; Newton, M. D.; Liu, Y.-P. *J. Am. Chem. Soc.* **1996**, *118*, 5221–5228. (d) Hanan, G. S.; Arana, C. R.; Lehn, J.-M.; Fenske, D. *Angew. Chem., Int. Ed. Engl.* **1995**, *34*, 1122–1124. (e) Baxter, P. N. W.; Hanan, G. S.; Lehn, J.-M. *Chem. Commun.* **1996**, 2019–2020. (f) Baxter, P. N. W.; Lehn, J.-M.; Fischer, J.; Youinou, M.-T. *Angew. Chem., Int. Ed. Engl.* **1994**, *33*, 2284–2287. (g) Dietrickbuecher, C. O.; Sauvage, J. *Chem. Rev.* **1987**, *87*, 795–810. (h) Balzani, V.; Credi, A.; Raymo, F. M.; Stoddart, J. F. *Angew. Chem., Int. Ed.* **2000**, *39*, 3348–3391. (i) Lawrence, D. S.; Jiang, T.; Levett, M. *Chem. Rev.* **1995**, *95*, 2229–2260. (j) Yashima, E.; Maeda, K.; Iida, H.; Furusho, Y.; Nagai, K. *Chem. Rev.* **2009**, *109*, 6102–6211. (k) Lehn, J.-M. *Supramolecular Chemistry*; VCH: Weinheim, Germany, 1995.
- (a) Serr, B. R.; Andersen, K. A.; Elliott, C. M.; Anderson, O. P. *Inorg. Chem.* **1988**, *27*, 4499–4504. (b) Youinou, M. T.; Ziessel, R.; Lehn, J. M. *Inorg. Chem.* **1991**, *30*, 2144–2148. (c) Albrecht, M.; Riether, C. *Chem. Ber.* **1996**, *129*, 829–832. (d) Goetz, S.; Kruger, P. E. *Dalton Trans.* **2006**, 1277–1284.
- (a) Enemark, E. J.; Stack, T. D. P. *Angew. Chem., Int. Ed. Engl.* **1995**, *34*, 996–998. (b) Albrecht, M.; Kotila, S. *Angew. Chem., Int. Ed. Engl.* **1995**, *34*, 2134–2137. (c) Kersting, B.; Meyer, M.; Powers, R. E.; Raymond, K. N. *J. Am. Chem. Soc.* **1996**, *118*, 7221–7222. (d) Meyer, M.; Kersting, B.; Powers, R. E.; Raymond, K. N. *Inorg. Chem.* **1997**, *36*, 5179–5191. (e) Albrecht, M.; Fröhlich, R. *J. Am. Chem. Soc.* **1997**, *119*, 1656–1661. (f) Albrecht, M.; Janser, I.; Houjou, H.; Fröhlich, R. *Chem.—Eur. J.* **2004**, *10*, 2839–2850.
- (a) Williams, A. F.; Piguet, C.; Bernardinelli, G. *Angew. Chem., Int. Ed. Engl.* **1991**, *30*, 1490–1492. (b) Charbonnière, L. J.; Bernardinelli, G.; Piguet, C.; Sargeson, A. M.; Williams, A. F. *J. Chem. Soc., Chem. Commun.* **1994**, 1419–1420. (c) Charbonnière, L. J.; Williams, A. F.; Frey, U.; Merbach, A. E.; Kamalipriya, P.; Schaad, O. *J. Am. Chem. Soc.* **1997**, *119*, 2488–2496. (d) Piguet, C.; Bernardinelli, G.; Bocquet, B.; Schaad, O.; Williams, A. F. *Inorg. Chem.* **1994**, *33*, 4112–4121.
- (a) Zhang, Z.; Dolphin, D. *Chem. Commun.* **2009**, 6931–6933. (b) Zhang, Z.; Dolphin, D. *Inorg. Chem.* **2010**, *49*, 11550–11555.
- (a) Piguet, C.; Bernardinelli, G.; Hopfgartner, G. *Chem. Rev.* **1997**, *97*, 2005–2062. (b) Knof, U.; von Zelewsky, A. *Angew. Chem.*

- Int. Ed.* **1999**, *38*, 302–322. (c) Albrecht, M. *Chem.—Eur. J.* **2000**, *6*, 3485–3489. (d) Albrecht, M. *Chem. Rev.* **2001**, *101*, 3457–3497. (e) Albrecht, M.; Fröhlich, R. *Bull. Chem. Soc. Jpn.* **2007**, *80*, 797–808. (f) Caulder, D. L.; Raymond, K. N. *J. Chem. Soc., Dalton Trans.* **1999**, 1185–1200.
- (7) Xu, J.; Parac, T. N.; Raymond, K. N. *Angew. Chem., Int. Ed.* **1999**, *38*, 2878–2882.
- (8) (a) Albrecht, M.; Kotila, S. *Chem. Commun.* **1996**, 2309–2310. (b) Scherer, M.; Caulder, D. L.; Johnson, D. W.; Raymond, K. N. *Angew. Chem., Int. Ed.* **1999**, *38*, 1587–1592. (c) Albrecht, M.; Blau, O.; Fröhlich, R. *Proc. Natl. Acad. Sci. U.S.A.* **2002**, *99*, 4867–4872. (d) Saalfrank, R. W.; Dresel, A.; Seitz, V.; Trummer, S.; Hampel, F.; Teichert, M.; Stalke, D.; Stadler, C.; Daub, J.; Schunemann, V.; Trautwein, A. X. *Chem.—Eur. J.* **1997**, *3*, 2058–2062.
- (9) (a) Sessler, J. L.; Gale, P. A.; Cho, W.-S. *Anion Receptor Chemistry*; Royal Society of Chemistry: Cambridge, U.K., 2006. (b) Katayev, E. A.; Ustynuk, Y. A.; Sessler, J. L. *Coord. Chem. Rev.* **2006**, *250*, 3004–3037. (c) Kang, S. O.; Begum, R. A.; Bowman-James, K. *Angew. Chem., Int. Ed.* **2006**, *45*, 7882–7894. (d) Caltagirone, C.; Gale, P. A. *Chem. Soc. Rev.* **2009**, *38*, 520–563. (e) Gale, P. A.; García-Garrido, S. E.; Garric, J. *Chem. Soc. Rev.* **2008**, *37*, 151–190. (f) Mullen, K. M.; Beer, P. D. *Chem. Soc. Rev.* **2009**, *38*, 1701–1713. (g) Steed, J. W. *Chem. Soc. Rev.* **2009**, *38*, 506–519. (h) Amendola, V.; Fabbrizzi, L. *Chem. Commun.* **2009**, 513–531.
- (10) Harding, L. P.; Jeffery, J. C.; Riis-Johannessen, T.; Rice, C. R.; Zeng, Z. *Dalton Trans.* **2004**, 2396–2397.
- (11) (a) Hasenknopf, B.; Lehn, J.-M.; Kneisel, B. O.; Baum, G.; Fenske, D. *Angew. Chem., Int. Ed. Engl.* **1996**, *35*, 1838–1840. (b) Hasenknopf, B.; Lehn, J.-M.; Boumediene, N.; Dupont-Gervais, A.; van Dorsselaer, A.; Kneisel, B. O.; Fenske, D. *J. Am. Chem. Soc.* **1997**, *119*, 10956–10962.
- (12) (a) Yang, X.; Knobler, C. B.; Hawthorne, M. F. *Angew. Chem., Int. Ed. Engl.* **1991**, *30*, 1507–1508. (b) Zheng, Z.; Knobler, C. B.; Hawthorne, M. F. *J. Am. Chem. Soc.* **1995**, *117*, 5105–5113.
- (13) Campos-Fernández, C. S.; Schottel, B. L.; Chifotides, H. T.; Bera, J. K.; Bacsá, J.; Koomen, J. M.; Russell, D. H.; Dunbar, K. R. *J. Am. Chem. Soc.* **2005**, *127*, 12909–12923.
- (14) (a) Fleming, J. S.; Mann, K. L. V.; Carraz, C.-A.; Psillakis, E.; Jeffery, J. C.; McCleverty, J. A.; Ward, M. D. *Angew. Chem., Int. Ed.* **1998**, *37*, 1279–1281. (b) Argent, S. P.; Riis-Johannessen, T.; Jeffery, J. C.; Harding, L. P.; Ward, M. D. *Chem. Commun.* **2005**, 4647–4649. (c) Paul, R. L.; Bell, Z. R.; Jeffery, J. C.; McCleverty, J. A.; Ward, M. D. *Proc. Natl. Acad. Sci. U.S.A.* **2002**, *99*, 4883–4888.
- (15) Hubner, G. M.; Glaser, J.; Seel, C.; Vogtle, F. *Angew. Chem., Int. Ed.* **1999**, *38*, 383–386.
- (16) (a) Jia, C.; Wu, B.; Li, S.; Yang, Z.; Zhao, Q.; Liang, J.; Li, Q.-S.; Yang, X.-J. *Chem. Commun.* **2010**, *46*, 5376–5378. (b) Jia, C.; Wu, B.; Li, S.; Huang, X.; Zhao, Q.; Li, Q.-S.; Yang, X.-J. *Angew. Chem., Int. Ed.* **2011**, *50*, 486–490. (c) Li, M.; Wu, B.; Jia, C.; Huang, X.; Zhao, Q.; Shao, S.; Yang, X.-J. *Chem.—Eur. J.* **2011**, *17*, 2272–2280. (d) Li, S.; Jia, C.; Wu, B.; Luo, Q.; Huang, X.; Yang, Z.; Li, Q.-S.; Yang, X.-J. *Angew. Chem., Int. Ed.* **2011**, *50*, 5721–5724. (e) Wu, B.; Yang, J.; Huang, X.; Li, S.; Jia, C.; Yang, X.-J.; Tang, N.; Janiak, C. *Dalton Trans.* **2011**, *40*, 5687–5696. (f) Zhuge, F.; Wu, B.; Liang, J.; Yang, J.; Liu, Y.; Jia, C.; Janiak, C.; Tang, N.; Yang, X.-J. *Inorg. Chem.* **2009**, *48*, 10249–10256. (g) Yang, Z.; Wu, B.; Huang, X.; Liu, Y.; Li, S.; Xia, Y.; Jia, C.; Yang, X.-J. *Chem. Commun.* **2011**, *47*, 2880–2882.
- (17) Sambrook, M. R.; Curriel, D.; Hayes, E. J.; Beer, P. D.; Pope, S. J. A.; Faulkner, S. *New J. Chem.* **2006**, *30*, 1133–1136.
- (18) Amendola, V.; Boiocchi, M.; Colasson, B.; Fabbrizzi, L.; Rodríguez Douton, M.-J.; Ugozzoli, F. *Angew. Chem., Int. Ed.* **2006**, *45*, 6920–6924.
- (19) (a) Perkins, D. F.; Lindoy, A.; McAuley, L. F.; Meehan, G. V.; Turner, P. *Proc. Natl. Acad. Sci. U.S.A.* **2006**, *103*, 532–537. (b) Persson, I.; Persson, P.; Sandstroem, M.; Ullstroem, A.-S. *J. Chem. Soc., Dalton Trans.* **2002**, 1256–1265, and references cited therein. (c) Otieno, T.; Blanton, J. R.; Hatfield, M. J.; Asher, S. L.; Parkin, S. *Acta Crystallogr., Sect. C: Cryst. Struct. Commun.* **2002**, *58*, m182–m185. (d) Deeth, R. J.; Hearnshaw, L. J. A. *Dalton Trans.* **2006**, 1092–1100.
- (20) Fenton, H.; Tidmarsh, I. S.; Ward, M. D. *Dalton Trans.* **2009**, 4199–4207.
- (21) Polin, J.; Schmohel, E.; Balzani, V. *Synthesis* **1998**, 321–324.
- (22) Uenishi, J.; Tanaka, T.; Nishiwaki, K.; Wakabayashi, S.; Oae, S.; Tsukubet, H. *J. Org. Chem.* **1993**, *58*, 4382–4388.
- (23) Sheldrick, G. M. *SADABS: Area-Detector Absorption Correction*; University of Göttingen: Göttingen, Germany, 1996.
- (24) Sheldrick, G. M. *SHELXS-97, SHELXL-97, Programs for Crystal Structure Analysis*; University of Göttingen: Göttingen, Germany, 1997.